51st AIAA Aerospace Sciences Meeting including the New Horizons Forum and Aerospace Exposition
07 - 10 January 2013, Grapevine (Dallas/Ft. Worth Region), Texas

AIAA 2013-0533

DNS of supersonic turbulent boundary layers over weakly and strongly adiabatic walls

Izaak B. Beekman*, Stephan Priebe†, M. Pino Martín‡

We present spatially developing direct numerical simulations (DNS) of turbulent boundary layers at Mach 3 and Mach 7 with $Re_\tau \approx 600$. In this work we make an explicit distinction in the wall thermal boundary condition, which, to our knowledge, has not been addressed in the literature. Namely, we deem "weakly adiabatic" walls as those whose temperature is fixed at the recovery temperature, and "strongly adiabatic" walls as those that enforce null heat transfer in the local and instantaneous sense. These two boundary conditions are bracketing cases for real materials that have finite, non-zero thermal diffusivities. Using scaling arguments, we propose a dimensionless quantity, the "fluctuation Nusselt number," as the relevant similarity parameter describing the thermal damping at the wall. Furthermore, we demonstrate that this parameter can vary by many orders of magnitude due to different thermal diffusivities of relevant wall materials and different edge Mach numbers. By design, the "weakly adiabatic" boundary condition damps near wall temperature fluctuations, which helps to enforce the assumption of weak total temperature fluctuations built into much of the theory for compressible boundary layers. Adopting a "strongly adiabatic" wall will place greater strain on these assumptions and may be more relevant to flight conditions of interest. Here we present data at Mach 3 for both boundary conditions, and at Mach 7 for the "strongly adiabatic" case. The simulations are spatially developing and have large domains to prevent unphysical forcing due to the inflow and spanwise boundary conditions, as discussed in Beekman, Priebe, Kan & Martin.[1] For all three data sets we present basic turbulence statistics and note that a non negligible effect is observed due to the differences in wall boundary condition.

I. Introduction

The existence of coherent vertical motions, or coherent structures, in boundary layers is now widely accepted. Theodorsen[2] postulated the existence of the hairpin vortex, a simple flow structure that explains the formation of low-speed streamwise streaks and the ejection of near-wall low-momentum fluid into higher-momentum regions farther from the wall. Head & Bandyopadhyay[3] provided experimental evidence of the streamwise stacking of individual hairpin vortices into larger structures, packets, whose heads describe an envelope inclined at a 15° to 20° downstream angle with respect to the wall. More recently, Adrian, Meinhart, & Tomkins[4] proposed a hairpin packet model, where the hairpins in a packet align in the streamwise direction as observed by Head and Bandyopadhyay. In this model, packets enclose regions of low momentum induced by their heads and counter-rotating legs, and align themselves in the streamwise direction giving rise to the low-momentum, very large-scale motions (VLSM) observed by Jiménez[5] and Kim & Adrian.[6] These long low-momentum streaks in the logarithmic region have also been observed by Hutchins & Marusic,[7] who call them "super structures." Recently Marusic and coworkers have proposed a model for the near wall streamwise fluctuations based on the observations studying superstructures.[8] This model displays remarkable Reynolds number independence and can accurately reproduce the near wall fluctuations, spectra and high order moments using information only obtained from the middle of the logarithmic region. In this model the presence of "super structures" influences the near wall fluctuations through two mechanisms: amplitude modulation of the high frequencies and superposition of the low frequency components.

*Graduate Student, Department of Mechanical and Aerospace Engineering, Princeton University. Visiting Graduate Student, Department of Aerospace Engineering, University of Maryland, College Park.
†Post-doctoral Research Associate, Department of Aerospace Engineering, University of Maryland, College Park.
‡AIAA Associate Fellow. Associate Professor, Department of Aerospace Engineering, University of Maryland, College Park.

The current study of the turbulence structure in boundary layers has been confined largely to the subsonic flow regime (e.g. Tomkins & Adrian;[9] del Álamo & Jiménez;[10] Ganapathisubramani, Longmire & Marusic;[11] del Álamo *et al.*;[12] del Álamo *et al.*;[13] Guala, Hommena & Adrian;[14] Hambleton, Hutchins & Marusic;[15] Flores *et al.*;[16] Balakumar & Adrian;[17] Hutchins & Marusic[7] and Mathis, Hutchins & Marusic[18]). The study of supersonic and hypersonic turbulent boundary layers has been primarily restricted to simple statistical analysis, due to the lack of detailed flow field data and the difficulty of performing experiments and simulations in this regime. Fernholz & Finley;[19,20] Spina, Donovan & Smits;[21] Smits & Wood;[22] Fernholz *et al.*;[23] and Smits & Dussauge,[24] give reviews including the effects of pressure gradient, streamline curvature and the interaction with shock waves in high-speed turbulent boundary layers. These descriptions are statistical and some include qualitative flow visualizations. The only structure information such as convection velocity, angle, and length scale, has been obtained from space-time correlations (see, for example, Smits *et al.*,[25] Spina, Donovan & Smits,[26] and Smits & Dussauge[24]). The results indicate changes in structure properties with both Mach and Reynolds numbers, such as a decrease in structure length with increasing Mach number.

Recent advances in numerical and experimental techniques allow for detailed four-dimensional–space and time–flow field data acquisition. Direct numerical simulations make possible the computation of turbulent boundary layers at supersonic and hypersonic Mach numbers (Guarini *et al.*;[27] Martin;[28,29] Pirozzoli, Grasso & Gatski;[30] Xu & Martin;[31] Ringuette, Wu & Martin[32]) as well as the interaction of turbulence with strong, unsteady shock waves (Adams;[33] Pirozzoli & Grasso;[34] Wu & Martin;[35] Wu & Martin;[36] Taylor, Grube & Martin;[37] Grube, Taylor & Martin[38]). Advanced particle-image-velocimetry techniques allow the temporal and spatial characterization of experimental supersonic turbulent boundary layers and shock boundary layer interactions (Elsinga *et al.*;[39]Schrijer, Scarano & van Oudheusden;[40] van Oudheusden;[41] Humble, Scarano & van Oudheusden[42]). Both numerical[35,32] and experimental[43,44,39] data at supersonic Mach numbers have shown evidence of VLSM.

Despite recent advances, there have been no simulations of adiabatic wall boundary layers which have employed a truly adiabatic wall in the traditional sense; to date many "adiabatic" simulations have been performed, however they are only adiabatic in the mean sense. Previous simulations, such as those by Duan, Beekman & Martin[45] and Pirozzoli & Bernardini,[46] have prescribed the wall temperature to be the recovery temperature. This "weakly adiabatic" boundary condition admits very large instantaneous and localized heat fluxes at the wall, which fluctuate about a zero mean. Furthermore, previous work by Duan, Beekman & Martin[47] has shown that changing the wall thermal boundary condition can have a large effect on the wall shear stress as well as the structure of the turbulence. Now this "weakly adiabatic" boundary treatment does have some advantages, chiefly it helps stabilize the allowable time step due to the CFL condition in comparison to the "strongly adiabatic" boundary condition where local wall temperature fluctuations will stiffen the simulation, driving down the time step. Furthermore, as we discuss below, this treatment may be a good proxy for certain steady state conditions, depending on the choice of model material. None the less, the alternative "strong" case warrants further consideration.

In this paper, we present the DNS of spatially developing Mach 3 and Mach 7 turbulent boundary layers over "weakly" and "strongly" adiabatic walls, as well as theoretical arguments as to the impact of these boundary conditions and their relevance to engineering applications. In addition, we propose a dimensionless similarity parameter to collapse the effect on the flow of a real wall's finite thermal diffusivity, and show that this parameter is a strong function of edge Mach number and wall material. Theoretical results and scaling arguments regarding the choice and effect of thermal wall boundary conditions are presented in Section II. The flow configuration and computational setup are described in Section III. In Section IV we present basic turbulence statistics for these three data sets, showing that our results are consistent with previous studies and that the impact of the different wall boundary conditions can be seen, even at Mach 3. Finally, conclusions and a discussion of future work are given in Section V.

II. Theoretical considerations

By dimensional analysis of the classic heat equation PDE, Equation 1, we note that the thermal diffusivity, $\alpha_s = \kappa_s/(\rho_s c_{p,s})$, is the correct quantity to describe the temporal response of a solid material to a given temperature gradient. Here, the "s" subscripts denote quantities associated with the solid wall, and its material properties. The thermal no-slip condition couples fluctuations and dissipation-events in the flow with the wall, imposing temporally and spatially fluctuating temperature gradient at the wall's surface. If, in the mean sense, the wall temperature is equal to the recovery temperature, then there will be no *mean* heat

flux to the wall, but the possibility of instantaneous heat transfer to–and within–the wall remains. If heat is transferred to the wall from the flow, this thermal energy must be transported within the wall in order to maintain zero-mean heat flux at the surface and conservation of energy. In the case of an infinite thermal diffusivity, corresponding to the "weakly adiabatic" boundary treatment, the wall or vehicle allows infinite local heat fluxes, which completely damp temperature fluctuations at the wall. Due to the kinematic no-slip condition, at the wall the static temperature is the total temperature, so it is also damped. Conversely, a zero thermal diffusivity corresponds to an infinitely insulated wall and the "strongly adiabatic" boundary condition. In this case no damping of total temperature will occur.

$$\frac{\partial T_s}{\partial t} = \alpha_s \nabla^2 T_s \tag{1}$$

As noted in the introduction, no detailed simulations of compressible wall boundary layers exist at the "strongly adiabatic" boundary condition. Additionally, most experiments are conducted with walls constructed of common metals such as brass, aluminum, copper or steel. All of these materials have relatively high thermal diffusivities, although significant variation still exists among them. Some vehicle materials, on the other hand, such as structural carbon-carbon composites (CCC) or ceramics have significantly lower thermal diffusivities. For example, the thermal diffusivities of some common lab-grade model materials, at typical lab stagnation temperatures, can be seen in Table 1. The values here are taken from Gustavsson *et al.*[48] The variation of over 300% among these values is not extreme but also non-negligible. On the other hand, the thermal diffusivities of some common, non ablating, flight-vehicle thermal protection systems, such as ceramics or CCCs can be many orders of magnitude lower. For example, Figure 1 shows plots of the thermal diffusivity of a sample CCC material from a NASA database of CCC thermal properties.[49] Note that the thermal diffusivity values of lab-grade materials listed in Table 1 and flight grade materials plotted in Figure 1 are in the same units, cm^2/s, but the CCC samples have thermal diffusivities 10 orders of magnitude smaller than the lab grade materials. Therefore, a representative range of boundary treatments should be investigated and an effective scaling developed. Due to the extreme variation in thermal diffusivities, even if the flow is a weak function of this boundary condition, its effects could still be important.

Material:	copper	aluminum	brass
Thermal diffusivity, α, $(cm^2 s^{-1})$:	1.09	0.65	0.33

Table 1. Thermal diffusivities of some common wind tunnel model materials at room temperature.[48]

We propose the dimensionless quantity, defined in Equation 2, as the appropriate similarity parameter to achieve this scaling. We call this parameter the "fluctuation Nusselt number." Traditionally, the Nusselt number is the ratio of the mean convective heat transfer coefficient of the fluid (including any conductive effects) to the mean conductive heat transfer coefficient of the solid at the boundary interface. As such, it describes which side of the interface is limiting or promoting heat transfer across the boundary. Here, our definition of the fluctuation Nusselt number is the ratio of the wall thermal diffusion timescale to the flows inner turbulent time scale. As the fluctuation Nusselt number tends to infinity, the wall can no longer adjust to the turbulence and the "strongly adiabatic" boundary condition approximation becomes true. As the fluctuation Nusselt number approaches zero, the wall allows for the instantaneous accommodation and damping of the thermal fluctuations in the flow at the wall-flow interface.

$$Nu^+ = \frac{\tau_{solid}}{\tau_{turbulence}} \tag{2}$$

By dimensional analysis of Equation 1, a characteristic length scale, in addition to the thermal diffusivity is required to formulate a time scale for the solid wall, $\tau_{solid} = \ell_s^2/\alpha_s$. For the turbulence time scale, we need an inner time scale that will reflect the frequency at which eddies exchange thermal energy with the wall through advection and viscous dissipation. For this case, we pick the viscous length scale, $z_\tau = \nu_w/u_\tau$ as our length scale and the friction velocity, $u_\tau = \sqrt{\tau_w/\rho_w}$ as the characteristic velocity scale. Together these form the usual inner viscous time scale, $\tau^+ = z_\tau/u_\tau$.

To help inform the choice of an appropriate length scale for the solid wall, let us first consider the motion of heat within the wall required to maintain conservation of energy and zero mean heat flux across the wall-fluid boundary. These modes of energy transport can be categorized into two conceptual types, where

a real solid wall will exhibit a combination of both modes simultaneously. The first mode is the capacitive mode: heat transfer only happens in the wall normal direction within the wall. Hot eddies or dissipation events will deposit their energy at a specific location, and a cold eddy, following at a later time, will travel over this hot-spot absorbing the previously deposited thermal energy back into the flow. The second mode of transport within the wall is the in-plane transport. Thermal energy will flow from a hot location to a neighboring cold location. Note that the thermal diffusivities of a composite wall material may be different for each of these modes as can be seen in Figure 1. The in-plane mode is significantly easier to conceptualize and explicitly treat, so here we assume that the capacitive mode's characteristic length varies proportionally to that of the in plane mode. Additionally, the in plane thermal diffusivity of composite materials tends to be greater than the through-the-thickness (t-t-t) thermal diffusivity.[49] Duan, Beekman & Martin[47,45] have found the spanwise, near wall streak spacing to be insensitive to Mach number and wall temperature, and to be approximately equal to the value of 100 viscous length scales commonly reported in the incompressible boundary layer literature.[24] This invariance suggests the characteristic in-plane length scale should be the viscous length scale. By including the appropriate time scales, equation 2 now becomes:

$$Nu^{+} = \frac{\tau_{solid}}{\tau_{turbulence}} \approx \frac{z_{\tau} u_{\tau}}{\alpha_s} = \frac{\overline{\nu_w}}{\alpha_s} \tag{3}$$

The advantage of this equation is that we can relate the kinematic viscosity at the wall to the edge Mach number. To do this, first we assume a power law relationship between viscosity and temperature, as seen in Equation 4. This formulation may be less accurate than Keye's viscosity law, or Sutherland's law over wide temperature ranges, but, locally, a power law is a decent approximation.[24,50] For air, at temperatures of interest $n \approx 3/4$.

$$\frac{\mu_w}{\mu_e} = \left(\frac{T_w}{T_e}\right)^{n} \tag{4}$$

Assuming zero mean pressure gradient in the wall normal direction, the equation of state yields a relationship between density and temperature across the boundary layer. Combining this with Equation 4, we now have a power law for the variation in kinematic viscosity across a boundary layer:

$$\frac{\nu_w}{\nu_e} = \left(\frac{T_w}{T_e}\right)^{(1+n)} \tag{5}$$

Now, taking the equation for the recovery temperature, a form of the total temperature equation accounting for viscous losses, and raising both sides to the exponent of Equation 5 yields an expression for the wall kinematic viscosity as a function of edge Mach number:

$$\frac{\nu_w}{\nu_e} = \left(\frac{T_w}{T_e}\right)^{(1+n)} = \left(1 + r\frac{\gamma - 1}{2} M_e^2\right)^{(1+n)} \tag{6}$$

Finally, rearranging Equation 6 and substituting into Equation 3, we find that the fluctuation Nusselt number goes as $M^{2(n+1)} \approx M^{7/2}$, where n is between 0.5 and 1. Therefore, the fluctuation Nusselt number is a strong function of Mach number. As the Mach number increases for a flow over a given wall material, the turbulence time scale rapidly becomes small relative to the wall conduction time scale. In this case, the instantaneous and mean mean heat flux at the wall approach zero, mimicking the "strongly adiabatic" boundary condition. Near wall enthalpy fluctuations are not damped under these circumstances, therefore greater total temperature fluctuations should exist in the near wall region, possibly leading to an increase in direct compressibility effects and straining the assumptions of theories such as Morkovin's hypothesis of weak compressibility.[24]

The fluctuation Nusselt number may vary substantially between vehicles, across the flight envelope of a given vehicle and between wind tunnel tests and the production vehicle if the model is made of different materials. Therefore, even a weak dependence of the turbulence on this parameter may produce very noticeable effects.

III. Flow configuration and computational details

The flow configuration considered in the present work is a spatially developing, zero pressure-gradient flat plate boundary layer over a smooth wall at Mach 2.9 and Mach 7.2. The domains are quite large, especially in

the streamwise direction, with a physical length of between 45 and 55 incoming boundary layer thicknesses. For the Mach 3 case, this length is about 0.4m. Over the domains the boundary layers approximately double in thickness. The edge conditions and usually boundary layer metrics can be seen below in Table 2. Note that the friction Reynolds number has been approximately fixed across the three cases. Values are listed for all three cases: Mach 3 "weakly adiabatic" (M3w), Mach 3 "strongly adiabatic" (M3s) and Mach 7 "strongly adiabatic" (M7s). All boundary layer quantities listed are taken at the rescaling station, which is approximately two boundary layer thicknesses upstream of the outlet, unless a range is specified, which corresponds to the range of values observed over the entire streamwise extent.

case	M_e	T_e (K)	T_w (K)	P (Pa)	Re_τ	Re_θ	δ_{99} (mm)	$\delta*$ (mm)	H
M3w	2.92	109	307	2361	650	5000	7.5 - 14	2.6 - 4.9	5.0
M3s	2.92	109	271	2361	600	5000	7.0 - 13	2.3 - 4.2	5.5
M7s	7.14	64.3	647	1413	560	17500	25 - 37	15 - 22	2.4

Table 2. Edge and boundary layer conditions of the three data sets. M3w: Mach 3, "weakly adiabatic;" M3s: Mach 3 "strongly adiabatic;" and M7s: Mach 7 "strongly adiabatic."

These conditions are representative of common laboratory conditions.[51] For the Mach 3 cases we use Sutherland's law to compute the viscosity, but the edge temperatures encountered in the Mach 7 case are below the temperature limits for accurate results using Sutherland's law, so here we adopt Keye's law.[50] Also note that the wall, in case M3w, is almost 40 K hotter than the true recovery temperature. This is due to a small drift in the edge conditions that occurs during the flow initialization process.

A table outlining the grid dimensions and resolution is given below in table 3. Here we use constant spacing in the streamwise, x, and spanwise, y, directions, and geometric grid stretching in the wall-normal, z, direction, where $z(k) = z_2(\alpha^{k-1} - 1)/(\alpha - 1)$. The grid spacing normalized by inner units is denoted as Δ^+. The domain length in a given direction is denoted by L/δ_0, where δ_0 is a reference boundary layer thickness. These grids are quite large, between approximately 150 Million points and 260 Million points, and they are run for more than 600 large eddy turnover timescales. Full volumes are output every 10 δ/U_e and select spanwise-wall-normal planes are output at high frequency for spectral analysis. Because of this, each data set about ten terabytes in size.

Case	δ_0 (mm)	L_x/δ_0	L_y/δ_0	Δ_x^+	Δ_y^+	z_2^+
M3w	6.41	60	5.0	9.2	3.5	0.26
M3s	6.41	60	10	8.1	3.2	0.28
M7s	2.04	54	9.0	7.1	2.7	0.27

Table 3. Grid resolution and domain size for the DNS. The grid is equispaced in the streamwise and spanwise directions and uses a geometric stretching in the wall normal direction. Here, $\delta_0 = 6.41$mm

The numerical scheme used here is identical to that used and validated by Martin[29,28] across multiple Mach numbers and wall temperature conditions. We use a 4th-order accurate, weighted essentially non-oscillatory (WENO) scheme, which has been linearly optimized.[52] The optimization process reduces the dissipation and dispersion in smooth regions by adding an additional candidate stencil and adjusting the optimal stencil weights, resulting in the linear portion of the scheme being nearly symmetric and bandwidth resolving efficiency optimized. For the spatial discretization of the viscous fluxes, 4th-order accurate central differencing is used, and time-integration is performed with a 3rd-order accurate, low-storage, explicit Runge-Kutta algorithm. The flow is initialized following the method of Martin.[29] The DNS code used here has been extensively validated across a wide range Mach numbers and wall temperatures, including those of the present study.[29]

The boundary conditions are as follows: For all cases a no-slip velocity boundary condition is used. A no-slip, isothermal boundary condition is used for the M3w case. Here, the prescribed wall temperature is 307K, which is close to the adiabatic wall temperature. For the M3s and M7s cases, $\partial T/\partial z = 0$ is enforced

at the wall every iteration. At the top and outlet boundaries, a supersonic exit boundary condition is used. In the spanwise direction, periodic boundary treatments are employed.

The inflow boundary condition is provided by the rescaling technique outlined by Xu & Martin.[31] This method has the advantage of being relatively simple to implement, all boundary variables are appropriately specified, and its action is well understood; we do not use any complicated reflection or shifting of the recycling plane. In our experience, when the DNS is run for long times (of the order of several hundreds of δ/U_∞), and a rescaling length typical of those commonly found in the literature is used, say 8δ, it becomes apparent that the rescaling forces an acoustic mode in the free-stream and can be clearly seen in time series spectra. This forcing is a narrow band phenomena at frequencies of U_c/λ_0 and higher harmonics. Here U_c is the applicable convection velocity, the local mean velocity, for instance, and λ_0 is the distance between the inflow plane and the recycling plane.

In addition to unphysical acoustic modes appearing in the free stream, the physics of the larger coherent structures may be artificially altered if the rescaling length is not sufficiently large. Large scale structures, which convect faster and change more slowly, are artificially reintroduced before they can sufficiently evolve. Previously,[1] we extended the analysis of Simens *et al.*,[53] regarding the Lagrangian eddy decorrelation time scale and its relation to an appropriate rescaling length for compressible boundary layers. We have used this analysis to inform our choice of inflow rescaling length for the present study.

IV. DNS data

In this section we examine basic turbulence quantities. We find our results are consistent with previous findings and that a moderate effect of the "weak" versus "strong" adiabatic boundary condition may be seen, even at Mach 3. Following the arguments outlined above, in Section II, we expect these discrepancies to increase with increasing Mach number. We have not yet finished computing the Mach 7 data set at the "weak" adiabatic boundary condition to verify this. In all the following figures case M3w will be plotted in blue, M3s in red, and M7s in black.

The coefficient of skin friction is plotted versus Reynolds number in Figure 2 for the Mach 3 cases and Figure 3 for the Mach 7 case. The smooth, solid line represents the theoretical relationship given by the van Driest II semi-empirical correlation. The smooth dashed lines represent this same relationship offset by the specified amount to fit the data. The DNS data have been temporally averaged over longer than $400\delta_0/U_e$ and in the spanwise direction, with no windowing or averaging in the streamwise direction. We clearly see a region near the inlet where the flow is recovering from the approximate inflow provided by the rescaling, but it quickly recovers and takes the functional form given by the van Driest II theory, with some offset from the prediction. The offset is within the range of previously cited values.[47,45,54,55] For the "strongly adiabatic" case this offset increases by 3% from the "weak" case. As the wall becomes thermally hardened and no longer damps the near wall enthalpy fluctuations, the skin friction increases. We plan to address the detailed mechanisms by which this occurs in future work.

This increase in skin friction also manifests itself in Figure 4. Here we have plotted the van Driest transformed velocity in inner units, versus the distance from the wall in inner units at numerous streamwise stations. Deviations in the skin friction will impact the additive constant associated with the log-law region, as can be seen. For the Mach 3 data, this additive constant is clearly a function of the wall boundary treatment, and we hypothesize that the Mach 7 case will follow a similar trend between the "weak" and "strong" cases. This deviation from the usual additive constant of 5.2 has been observed before, when manipulating the wall thermal boundary condition.[47,54]

For the "strongly adiabatic" boundary condition it is also possible to empirically compute a recovery factor, rather than assuming one *a priori*. This provides another check of the validity of our data, and the extent and impact of the inflow boundary condition. As can be seen in Figure 5, our computed recovery factor of 0.89 agrees very well with the values previously reported.[24] There is a limited region near the inlet where the flow is perturbed from the rescaling procedure, but the recovery factor quickly relaxes back to the accepted value. Additionally it appears that this quantity may be a very weak function of Mach number.

In addition, the Reynold's shear stresses match previously observed values and display no unexpected behavior. Figure 6(a) plots the Reynolds shear stresses of the current simulations and Figure 6(b) has been reproduced from Duan, Beekman & Martin 2011 which includes data at nearly the same conditions.[45] The location and magnitude of the inner peak values of Reynolds shear stress match quite closely.

V. Conclusions and future work

We have provided theoretical arguments as to why an additional boundary treatment should be investigated, the "strongly adiabatic" wall in addition to the previously simulated "weakly adiabatic" wall boundary condition. Real materials will behave as some unknown combination of these two boundary conditions, but each on its own will bracket the entire range of behaviors. In order that this effect be correctly studied and parametrized, we derive a similarity parameter, the fluctuation Nusselt number, which we hypothesize to be the correct quantity to collapse data across different wall and free-stream conditions. Furthermore, because of its nearly quartic dependence on edge Mach number, and the extreme variation possible in the thermal diffusivity of wall materials, this similarity parameter may vary over many orders of magnitude. Therefore, even if the turbulence behavior is a weak function of fluctuation Nusselt number, non-negligible effects may be observed due to this extreme variation.

The data sets for both wall conditions at Mach 3 and for the "strong" condition at Mach 7 are consistent with previous observations. A shift in the wall skin friction and the additive constant in the streamwise velocity log layer was observed between the two boundary conditions at Mach 3, and similar behavior has been seen before when varying the wall temperature of isothermal walls.[47,54]

However, to obtain a detailed understanding of the underlying mechanisms of these differences further work is needed. For the basis of comparison, a Mach 7 "weakly adiabatic" simulation is currently being run, as well as an incompressible reference case at a matching Reynolds number. Furthermore, to asses any direct compressibility effects which may be introduced by the removal of the near wall total temperature fluctuations, turbulence kinetic energy budgets should be computed. To assess any change in turbulence structure and the underlying physical mechanism which may account for discrepancies between the two flows, instantaneous realizations should be analyzed as well as statistical structure data, such as wave number and frequency spectra and two point correlations and convection velocities. We plan to accomplish this analysis in a future publication.

Acknowledgments

This work is supported by the Air Force Office of Scientific Research under grant AF/9550-10-1-0535 STW 21 - Revitalization of the hypersonics testing and evaluation workforce.

References

[1]Beekman, I. B., Priebe, S., and Martin, M. P., "DNS of a Large-Domain, Mach 3 Turbulent Boundary Layer: Turbulence Structure," *AIAA Paper 2011-0753*, 2011.

[2]Theodorsen, T., "Mechanism of Turbulence," *Proc. 2nd. Midwestern Conf. on Fluid Mech.*, Ohio State University, Columbus, Ohio, USA, 1952, pp. 1–19.

[3]Head, M. and Bandyopadhyay, P., "New aspects of turbulent boundary-layer structure," *J. Fluid Mech.*, Vol. 107, 1981, pp. 297–338.

[4]Adrian, R., Meinhart, C., and Tomkins, C., "Vortex organization in the outer region of the turbulent boundary layer," *J. Fluid Mech.*, Vol. 422, 2000, pp. 1–54.

[5]Jiménez, J., "The largest scales of turbulent wall flows," *Center for Turbulence Research, Annual Research Briefs*, Stanford University, 1998, pp. 137–154.

[6]Kim, K. C. and Adrian, R. J., "Very large-scale motion in the outer layer," *Phys. Fluids*, Vol. 11, No. 2, 1999, pp. 417–422.

[7]Hutchins, N. and Marusic, I., "Evidence of very long meandering features in the logarithmic region of turbulent boundary layers," *J. of Fluid Mechanics*, Vol. 579, 2007, pp. 1–28.

[8]Marusic, I., Mathis, R., and Hutchins, N., "Predictive model for wall-bounded turbulent flow," *Science*, Vol. 329, No. 5988, 2010, pp. 193–196.

[9]Tomkins, C. and Adrian, R., "Spanwise structure and scale growth in turbulent boundary layers," *J. Fluid Mech.*, Vol. 490, 2003, pp. 37–74.

[10]del Álamo, J. C. and Jiménez, J., "Spectra of the very large anisotropic scales in turbulent channels," *Phys. Fluids*, Vol. 15, No. 6, 2003, pp. L41–L44.

[11]Ganapathisubramani, B., Longmire, E. K., and Marusic, I., "Characteristics of vortex packets in turbulent boundary layers," *J. Fluid Mech.*, Vol. 478, 2003, pp. 35–46.

[12]del Álamo, J. C., Jiménez, J., Zandonade, P., and Moser, R. D., "Scaling of the energy spectra of turbulent channels," *J. Fluid Mech.*, Vol. 500, 2004, pp. 135–144.

[13]del Álamo, J. C., Jiménez, J., Zandonade, P., and Moser, R. D., "Self-similar vortex clusters in the turbulent logarithmic region," *J. Fluid Mech.*, Vol. 561, 2006, pp. 329–358.

[14]Guala, M., Hommema, S. E., and Adrian, R. J., "Large-scale and very-large-scale motions in turbulent pipe flow," *J. Fluid Mech.*, Vol. 554, 2006, pp. 521–542.

[15]Hambleton, W. T., Hutchins, N., and Marusic, I., "Simultaneous orthogonal-plane particle image velocimetry measurements in a turbulent boundary layer," *J. Fluid Mech.*, Vol. 560, 2006, pp. 53–64.

[16]Flores, O., Jiménez, J., and del Álamo, J. C., "Vorticity organization in the outer layer of turbulent channels with disturbed walls," *J. Fluid Mech.*, Vol. 591, 2007, pp. 145–154.

[17]Balakumar, B. J. and Adrian, R. J., "Large- and very-large-scale motions in channel and boundary-layer flows," *Phil. Trans. R. Soc. A*, Vol. 365, 2007, pp. 665–681.

[18]Mathis, R., Hutchins, N., and Marusic, I., "Large-scale amplitude modulation of the small-scale structures in turbulent boundary layers," *J. Fluid Mech.*, Vol. 628, 2009, pp. 311–337.

[19]Fernholz, H. H. and Finley, P. J., "A critical commentary on mean flow data for two-dimensional compressible turbulent boundary layers," *AGARDograph 253*, 1980.

[20]Fernholz, H. H. and Finley, P. J., "A further compilation of compressible turbulent boundary layer data with a surveyof turbulence data," *AGARDograph 263*, 1981.

[21]Spina, E., Smits, A., and Robinson, S., "The physics of supersonic turbulent boundary layers," *J. Fluid Mech.*, Vol. 26, 1994, pp. 287–319.

[22]Smits, A. and Wood, D., "The response of turbulent boundary layers to sudden perturbations," *Annual Review of Fluid Mechanics*, Vol. 17, 1985, pp. 321–358.

[23]Fernholz, H. H., Smits, A., Dussauge, J., and Finley, P., "A survey of measurements and measuring techniques in rapidly distorted compressible turbulent boundary layers," *AGARDograph 315*, 1989.

[24]Smits, A. J. and Dussauge, J.-P., *Turbulent shear layers in supersonic flow*, Springer, 2nd ed., 2006.

[25]Smits, A., Spina, E., Alving, A., Smith, R., Fernando, E., and Donovan, J., "A comparison of the turbulence structure of subsonic and supersonic boundary layers," *Phys. Fluids A*, Vol. 1, 1989, pp. 1865–1875.

[26]Spina, E., Donovan, J., and Smits, A., "On the structure of high-Reynolds number supersonic turbulent boundary layers," *J. Fluid Mech.*, Vol. 222, 1991, pp. 293–327.

[27]Guarini, S., Moser, R., Shariff, K., and Wray, A., "Direct numerical simulation of supersonic turbulent boundary layer at Mach 2.5," *J. of Fluid Mech.*, Vol. 414, 2000, pp. 1–33.

[28]Martín, M. P., "DNS of hypersonic turbulent boundary layers," *AIAA Paper 2004-2337*, 2004.

[29]Martín, M. P., "Direct numerical simulation of hypersonic turbulent boundary layers. Part 1: Initialization and comparison with experiments," *J. Fluid Mech.*, Vol. 570, 2007, pp. 347–364.

[30]Pirozzoli, S., Grasso, F., and Gatski, T., "Direct numerical simulation and analysis of a spatially evolving supersonic turbulent boundary layer at M=2.25," *Phys. Fluids*, Vol. 16, No. 3, 2004, pp. 530–545.

[31]Xu, S. and Martín, M., "Assessment of Inflow Boundary Conditions for Compressible Turbulent Boundary Layers," *Physics of Fluids*, Vol. 16, No. 7, 2004, pp. 2623–2639.

[32]Ringuette, M. J., Wu, M., and Martín, M. P., "Coherent structures in direct numerical simulation of turbulent boundary layers at Mach 3," *J. Fluid Mech.*, Vol. 594, 2008, pp. 59–69.

[33]Adams, N., "Direct simulation of the turbulent boundary layer along a compression ramp at $M = 3$ and $Re_\theta = 1685$," *J. of Fluid Mech.*, Vol. 420, 2000, pp. 47–83.

[34]Pirozzoli, S. and Grasso, F., "Direct numerical simulation of impinging shock wave/turbulent boundary layer interaction at M=2.25," *Phys. Fluids*, Vol. 18, No. 6, 2006.

[35]Wu, M. and Martín, M., "Direct numerical simulation of shockwave and turbulent boundary layer interactions over a compression ramp," *AIAA J.*, Vol. 45, 2007, pp. 879–889.

[36]Wu, M. and Martín, M., "Analysis of shock motion in shockwave and turbulent boundary layer interaction using direct numerical simulation data," *J. of Fluid Mechanics*, Vol. 594, 2008, pp. 71–83.

[37]Taylor, E. M., Grube, N., and Martín, M. P., "Evaluation of traditional and shock-confining LES filters using data of compressible turbulence," *AIAA Paper Number 2007-4197*, 2007.

[38]Grube, N., Taylor, E. M., and Martín, M. P., "Numerical Investigation of Shock/Isotropic Turbulence Interactions," *49th AIAA Aerospace Sciences Meeting including the New Horizons Forum and Aerospace Exposition. Orlando, Florida. Jan 4 - 7*, 2011.

[39]Elsinga, G., Adrian, R., Van Oudheusden, B., and Scarano, F., "Three-dimensional vortex organization in a high-Reynolds-number supersonic turbulent boundary layer," *J. of Fluid Mech.*, Vol. 644, 2010, pp. 35–60.

[40]Schrijer, F., Scarano, F., and van Oudheusden, B., "Application of PIV in a Mach 7 double-ramp flow," *Experiments in Fluids*, Vol. 41, 2006, pp. 353–363.

[41]van Oudheusden, B., "Principles and application of velocimetry-based planar pressure imaging in compressible flows with shocks," *Experiments in Fluids (electronic Open Access)*, 2008.

[42]Humble, R., Scarano, F., and van Oudheusden, B., "Experimental study of an incident shock wave/turbulent boundary layer interaction using PIV," *AIAA Paper Number*, Vol. number 2006-3361, 2006.

[43]Ganapathisubramani, B., Clemens, N., and Dolling, D., "Large-scale motions in a supersonic turbulent boundary layer," *J. Fluid Mech.*, Vol. 556, 2006, pp. 1–11.

[44]Ganapathisubramani, B., Clemens, N., and Dolling, D., "Effects of upstream boundary layer on the unsteadiness of shock-induced separation," *J. Fluid Mech.*, Vol. 585, 2007, pp. 369–394.

[45]Duan, L., Beekman, I., and Martin, M., "Direct numerical simulation of hypersonic turbulent boundary layers. Part 3. Effect of Mach number," *J. Fluid Mech.*, Vol. 672, 2011, pp. 245–267.

[46]Pirozzoli, S. and Bernardini, M., "Turbulence in supersonic boundary layers at moderate Reynolds number," *J. Fluid Mech.*, Vol. 688, 2011, pp. 120–168.

[47]Duan, L., Beekman, I., and Martin, M., "Direct numerical simulation of hypersonic turbulent boundary layers. Part 2. Effect of wall temperature," *J. Fluid Mech.*, Vol. 655, 2010, pp. 419–445.

[48]Gustavsson, M., Karawacki, E., and Gustafsson, S., "Thermal conductivity, thermal diffusivity and specific heat of thin samples from transient measurements with hot disk sensors," *Rev. Sci. Insrum*, Vol. 65, No. 12, 1994, pp. 3856–3859.

[49]Ohlhorst, C., Vaughn, W., Ransone, P., and Tsou, H., "Thermal Conductivity Database of Various Structural Carbon-Carbon Composite Materials," Tech. rep., NASA Technical Memorandum 4787, 1997.

[50]Roy, C. and Blottner, F., "Review and Assessment of Turbulence Models for Hypersonic Flows," *Progress in Aerospace Sciences*, Vol. 42, 2006, pp. 469–530.

[51]Williams, O. and Smits, A., "Application of PIV to the Measurement of Hypersonic Turbulence," *16th Int. Symp. on Applications of Laser Techniques to Fluid Mechanics*, 2012.

[52]Martin, M. P., Taylor, E. M., Wu, M., and Weirs, V. G., "A Bandwidth-Optimized WENO Scheme for the Direct Numerical Simulation of Compressible Turbulence," *J. of Comp. Physics*, Vol. 220, 2006, pp. 270–289.

[53]Simens, M., Jimnez, J., Hoyas, S., and Mizuno, Y., "A high-resolution code for turbulent boundary layers," *J. of Comp. Physics*, Vol. 228, No. 11, 2009, pp. 4218–4231.

[54]Maeder, T., Adams, N., and Kleiser, L., "Direct simulation of turbulent supersonic boundary layers by an extended temporal approach." *J. Fluid Mech.*, Vol. 429, 2001, pp. 187–216.

[55]Maeder, T., *Numerical investigation of supersonic turbulent boundary layers.*, Ph.D. thesis, ETH, Zürich, 2000.

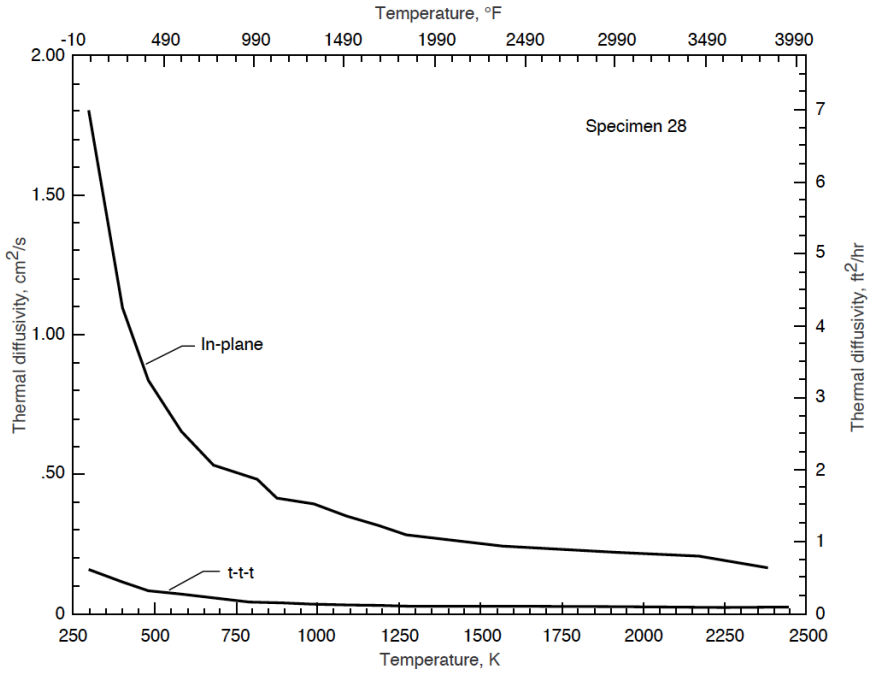

Figure 1. A representative plot of the through-the-thickness (t-t-t) and in-plane thermal diffusivities of structural carbon-carbon composite materials from NASA technical memorandum 4787.[49] These values are many orders of magnitude smaller than those for many common wind tunnel model materials.

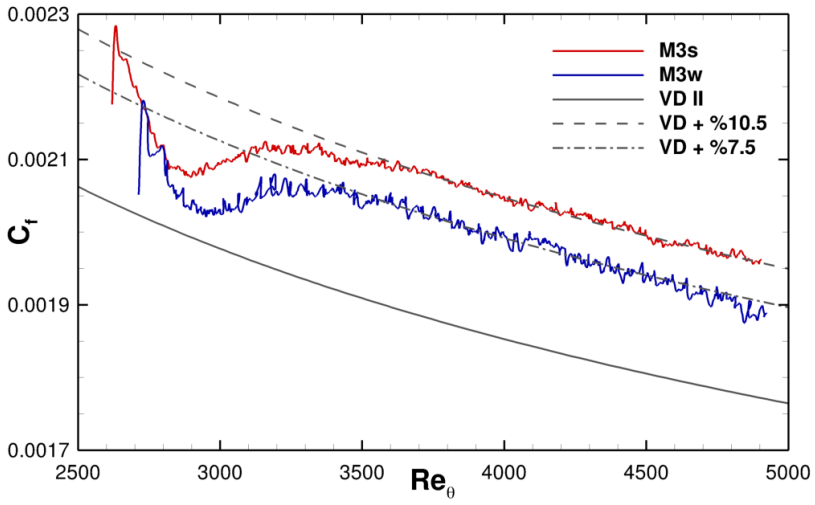

Figure 2. Comparison of the Mach 3 data sets against the van Driest II semi-empirical theory. The dashed lines are the predictions adjusted by a constant percentage to fit the data. A variation of 3% is visible between the "strong" and "weak" cases. The data have been averaged temporally over 400+ large eddy turn over times and in the spanwise direction. No streamwise windowing or averaging has been performed.

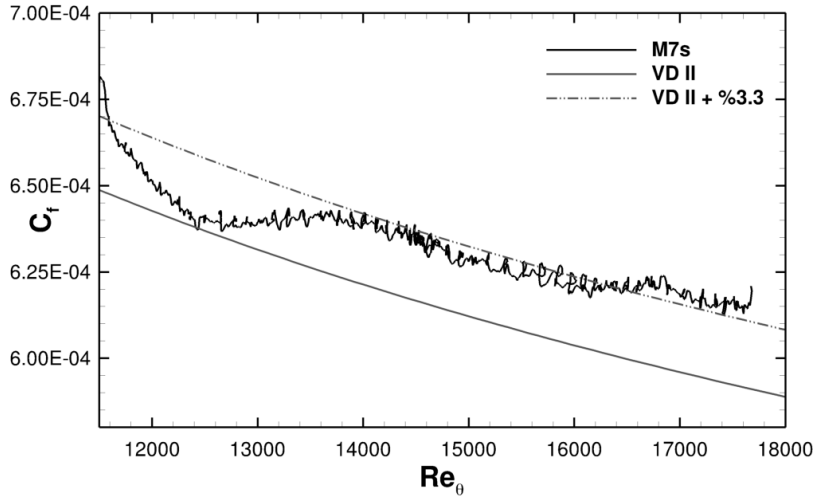

Figure 3. The Mach 7 data set and the semi-empirical van Driest II prediction. The dashed line is offset by 3.3% to fit the data. As in the Mach 3 data above, the influence of the rescaling technique can be seen in the first portion of the domain, but the flow quickly relaxes back to equilibrium.

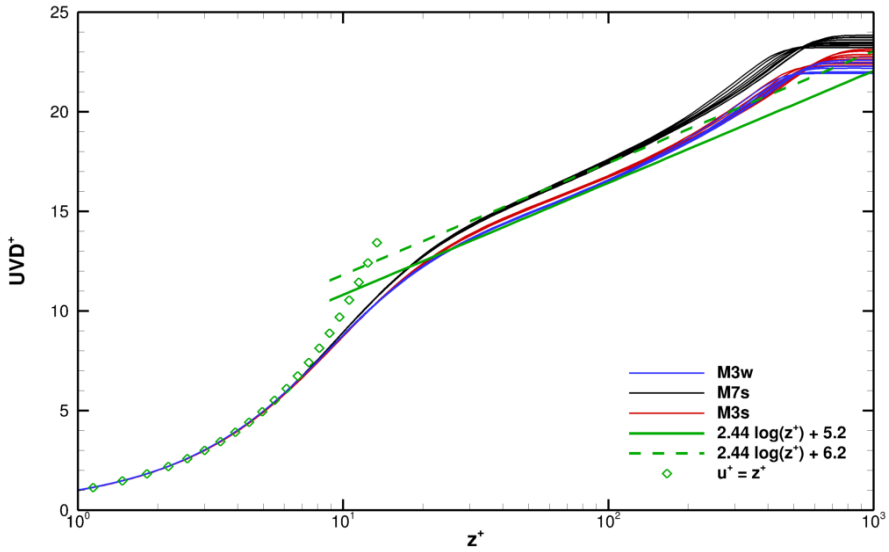

Figure 4. Van Driest transformed velocity profiles for all three cases plotted in inner units on a linear-log scale. For each case multiple streamwise locations are plotted and the variation of Reynolds number with down-stream location is evident. A modification of the additive log-law constant is present for the "strong" cases with mild variation at Mach 3 and larger variation at Mach 7.

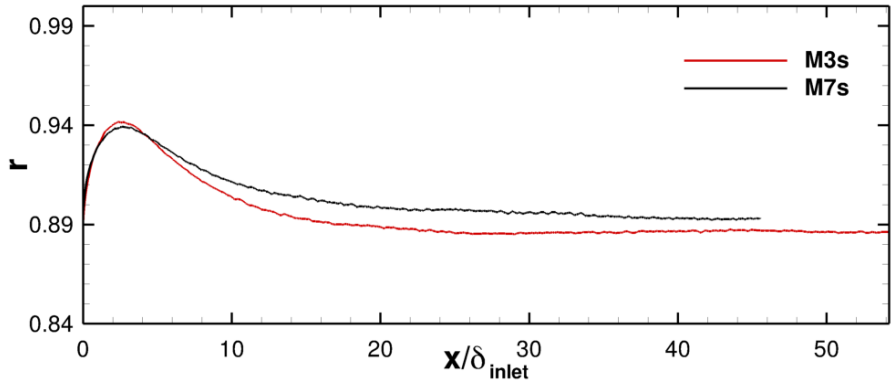

Figure 5. The empirically calculated recovery factor for the Mach 3 and Mach 7 "strong" case. The value of 0.89 is in excellent agreement with previous observations.[24] As in the skin friction coefficient, the spatial transient associated with the inflow specification is evident, before it quickly re-equilibrates. Some mild variation with Mach number may exist.

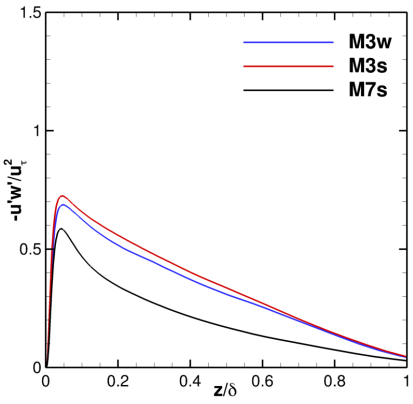

(a) Reynolds shear stresses of the current data sets.

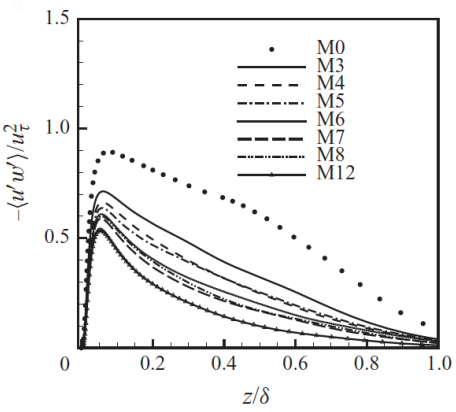

(b) Reynolds shear stresses at various Mach numbers from Duan, Beekman & Martin.[45]